# Total reaction and neutron-removal cross sections of $(30-60)A$ MeV He and Li isotopes on Pb

R. E. Warner,[1] M. H. McKinnon,[1] N. C. Shaner,[1] F. D. Becchetti,[2] A. Nadasen,[3] D. A. Roberts,[2] J. A. Brown,[4] A. Galonsky,[5] J. J. Kolata,[6] R. M. Ronningen,[5] M. Steiner,[5] and K. Subotic[7]

[1]*Oberlin College, Oberlin, Ohio 44074*

[2]*University of Michigan, Ann Arbor, Michigan 48109*

[3]*University of Michigan, Dearborn, Michigan 48128*

[4]*Millikin University, Decatur, Illinois 62522*

[5]*National Superconducting Cyclotron Laboratory, East Lansing, Michigan 48824*

[6]*University of Notre Dame, Notre Dame, Indiana 46556*

[7]*Institute of Nuclear Sciences, VINCA, Belgrade 11001, Yugoslavia*

(Received 19 January 2000; revised manuscript received 20 March 2000; published 19 July 2000)

Total reaction cross sections $\sigma_R$ of $(30-60)A$ MeV $^{4,6,8}$He and $^{6,7,8,9,11}$Li on Pb, and $2n$-removal cross sections $\sigma_{-2n}$ of $^{6,8}$He and $^{11}$Li on Pb, were measured by injecting magnetically separated, focused, monoenergetic, secondary beams of those projectiles into a telescope containing Pb targets separated by thin Si detectors. All these $\sigma_R$'s (except $^4$He), and $\sigma_{-2n}$ for $^6$He and $^{11}$Li, are underpredicted by microscopic model calculations which include only nuclear forces. Better agreement is achieved by including electromagnetic dissociation in the model, for those projectiles for which either the electric dipole response functions or the dominant photodissociation cross sections were known. The cross sections $\sigma_{-4n}$ for $^8$He, $\sigma_{-xn}$ for $^{7,8,9}$Li, and $(\sigma_{-3n}+\sigma_{-4n})$ for $^{11}$Li were found to be $\leqslant 0.7$ b. All $\sigma_R$'s were measured to better than 5% accuracy, showing that the method is usable for other target elements sandwiched into a Si telescope.

PACS number(s): 25.60.Dz, 24.10.−i

## I. INTRODUCTION

During the last decade we measured total reaction cross sections $\sigma_R$ and one- or two-nucleon removal cross sections $\sigma_{-xN}$ for many light projectiles ($A=2-17$) incident upon silicon detectors used as active targets. The projectiles included the $2n$-halo nuclei $^6$He and $^{11}$Li [1] and the proton-halo candidates $^8$B, $^{12}$N, and $^{17}$Ne [2], at energies up to about 60 MeV/nucleon. These measurements are intended to test nuclear models and get information about projectile matter distributions including, in some cases, their halo structure.

The best fits to our data were obtained from a microscopic (Glauber) model [3], though strong absorption and conventional optical model fits (where parameters were available) were also attempted. The microscopic model starts from known nucleon-nucleon interaction cross sections $\sigma_{NN}$ and assumed matter distributions. It finds the reaction probability in an elementary volume where projectile and target overlap, and integrates this probability over the nuclear volumes, the trajectory, and all impact parameters. At energies below 100 MeV/nucleon the model is relatively insensitive to $\sigma_{NN}$; the latter is so large that, on orbits with impact parameters less than the strong interaction radius, reactions nearly always occur. Thus the model becomes particularly appropriate for testing nuclear matter distributions. While the model was first applied to high-energy data [3], it works surprisingly well even for energies of a few MeV/nucleon for Si targets [4], on which most reactions are caused by nuclear rather than Coulomb forces.

A remaining question is the model's utility at low and medium energies for heavy targets, for which electromagnetic dissociation (EMD) is a prominent effect. The existing $\sigma_R$ and $\sigma_{-xN}$ data for $^{11}$Li+Pb at energies below 100 MeV/nucleon agree less well with the theory than do higher-energy data [5–9]. Therefore we have now measured $\sigma_R$ and $\sigma_{-xN}$ for most bound He and Li isotopes on Pb, at energies up to about 60 MeV/nucleon, and we compare them with model predictions.

In previous measurements [1,2], secondary beams of the projectiles of interest were injected into, and stopped in, a telescope containing only Si detectors. Total energy-deposit spectra were observed, and projectiles which had energy losses other than those expected from ionization alone were identified as reacting. Further, those with appropriate energy deficits (e.g., $\frac{2}{11}$ of the incident energy for $^{11}$Li) could be identified as $2n$-removal reactions. The use of a series of Si detectors provided measurements in different projectile energy ranges, giving information about the energy dependence of $\sigma_R$ and $\sigma_{-xN}$. In the present measurements, Pb targets were placed between the Si detectors in a telescope and the Si background, known from earlier measurements [1], was subtracted.

Section II of this paper describes the experimental procedure, including the identification of reactions. Unlike the earlier measurements, there are large unmeasured energy losses in the targets of interest, requiring new data analysis techniques. These are described in Sec. III, where we show how $\sigma_R$ and $\sigma_{-xN}$ are deduced from the reaction yields. Section IV presents microscopic model calculations, showing that the data are reasonably well fitted by this model only in those cases where we can include EMD effects. Section V contains our conclusions.

## II. EXPERIMENTAL PROCEDURE

The projectiles were produced at the National Superconducting Cyclotron Laboratory by fragmentation of a primary

 

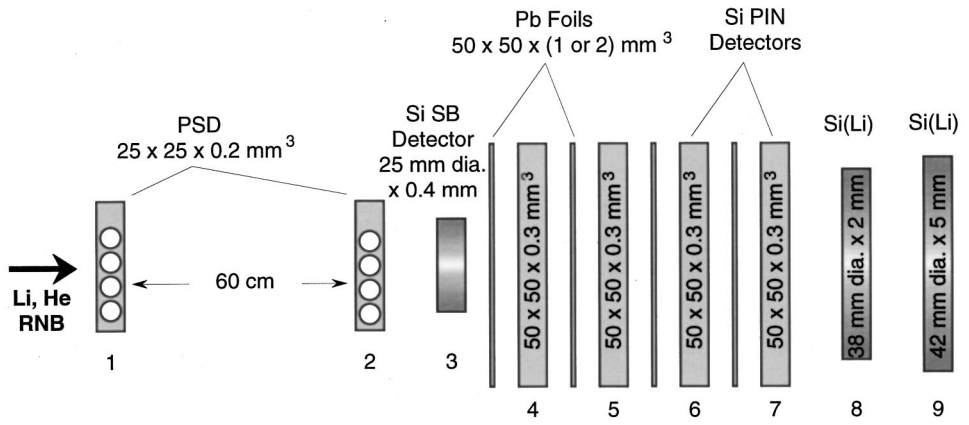


FIG. 1. Si detector and Pb target telescope (not to scale) used in this experiment.

80*A* MeV $^{18}$O beam, up to 50 pnA in intensity, incident upon a 0.75 gm/cm$^2$ Be target at the entrance to the *A*1200 analyzing system. An achromatic Al wedge, placed in an intermediate image plane, reduced their energy while preserving their momentum resolution. Finally, the system focused the secondary beams on the telescope shown in Fig. 1. The energies for $^4$He and $^6$Li were chosen so that they stopped halfway through detector 8; other beams stopped halfway through detector 9.

As in the earlier work [1], anomalous signals from the Si detectors identified those projectiles of interest which underwent reactions. Unlike those earlier experiments, the intended targets were Pb sheets, 1.9 mm thick for the He beams and 1 mm thick for the Li beams, placed between detectors.

The first two (position-sensitive) detectors selected a beam of 6 mm radius; their energy-loss signals rejected beam contaminants. Detector 1 was about 60 cm upstream from detector 2. The remaining components were close packed, with detector 9 about 17 cm from detector 2.

The reactions were of two basic types, requiring separate identification methods. Those where the projectile changed its atomic number in a given detector (''*Z* changing''), or in the preceding Pb target, generally gave anomalous pulses in that detector. However, neutron-removal reactions produced charged fragments which traversed one or two detectors before their signals could be distinguished from those of nonreacting projectiles.

Examples of fragment groups from *n*-removal reactions appear in Figs. 2 and 3, which are event plots of energy loss in detector 7 vs the combined losses (E89) in detectors 8 and 9. Detector energy calibrations were obtained from detector thicknesses and the ionizing powers [10] and pulse heights of nonreacting projectiles. The fragments were identified using the algorithm

$$R = aE^p, \tag{1}$$

where $R$ and $E$ are the range and energy, and $p \simeq 1.78$ empirically gave optimum resolution of particle groups.

Figure 2 shows an intense group of $\alpha$ particles from $^6$He dissociation. Nearly all nonreacting $^6$He projectiles have $E_7 \approx 5.5$ MeV and $E_{89} \approx 140$ MeV, but there are three additional categories. Those below the main group, less than 1% of the total, have channeled in detector 7; those to its right represent pileup. Energy-degraded $^6$He's appear above and to the left; their number can be explained by energy straggling throughout the telescope but must include some inelastic scattering events. Events in the band marked $\Delta E_7$ react in detectors 8 or 9 after avoiding reactions in preceding elements; we call these events the ''normal-$\Delta E_7$ band.'' Reaction products with $Z=1$ appear near the origin. Many reactions (not shown), at the origin or on the vertical axis, have products which stop before or in detector 7.

Figure 3, for incident $^{11}$Li, shows similar features. The most intense reaction group, as expected, is $^9$Li. Multineutron removal to $^{7,8}$Li, as well as particle groups with $Z=1$ (near the origin) and $Z=2$ are observed. $^{11}$Li, unlike $^6$He, shows a resolved low-energy group of nonreacting projectiles, making up about 0.1% of the beam. We verified that their signals could not simulate reactions, but nevertheless we rejected these events during analysis. No other projectiles showed this apparent beam defect.

Energy spectra of identified $^4$He from $^6$He dissociation, and $^9$Li from $^{11}$Li dissociation, are shown in Figs. 4 and 5, respectively. In both cases, some fragments formed in the

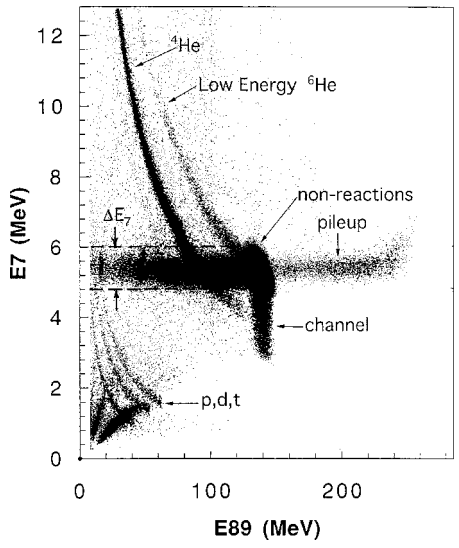


FIG. 2. Two-dimensional particle spectra from the last three detectors, with 64 MeV/nucleon $^6$He incident upon the telescope shown in Fig. 1.

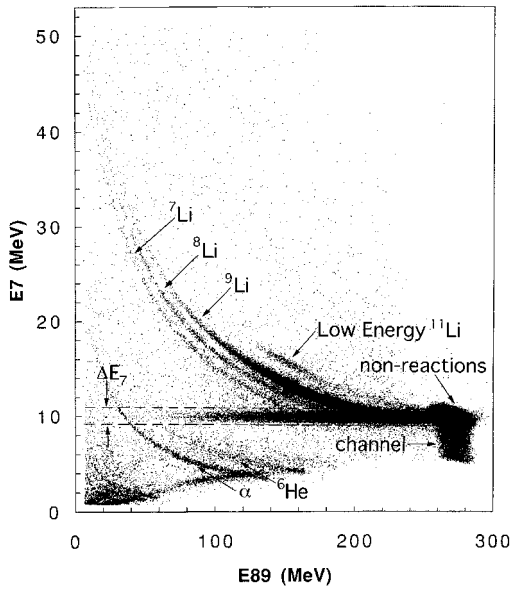


FIG. 3. Similar to Fig. 2, for 56 MeV/nucleon incident $^{11}$Li.

final Pb target entered detector 7 with ionizing powers similar to nonreacting projectiles, and were lost in the normal-$\Delta E_7$ band. All events in this band were rejected by software gates; later we estimate, and correct for, the number of rejected $2n$-removal events which should be counted.

Other reaction events, mainly $Z$-changing except for some $n$-removal events occurring early in the telescope, were identified in the one-dimensional energy spectra of detectors 3–7.

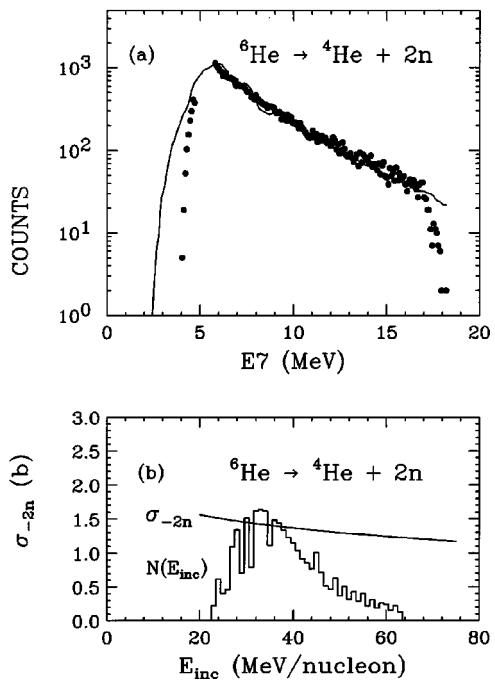


FIG. 4. (a) Spectrum in detector 7 of identified $^4$He with energies above the $\Delta E_7$ band (see Fig. 2), from incident $^6$He. The histogram shows the model predictions described in text. (b) Model predictions of $\sigma_{-2n}$, and spectrum of energies at which $^6$He's dissociate producing the fragments detected in this experiment.

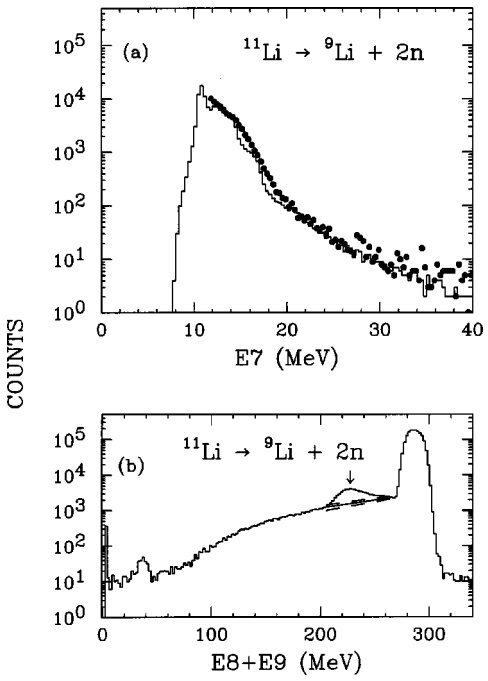


FIG. 5. (a) Similar to Fig. 4(a), for $^9$Li fragments from $^{11}$Li. (b) Summed energies in last two detectors for events in the $\Delta E_7$ band (Fig. 3) showing enhancement due to neutron-removal. Solid and dashed lines show deduced $n$-removal yield and its uncertainty.

For example, Fig. 6(a) shows the total event spectrum of detector 7 for incident $^9$Li, after rejection of $n$-removal and pileup events by software gates. The peak near 10 MeV, due to nonreacting projectiles, has a low-energy shoulder due to channeling in this detector. To obtain the reaction yield spectrum it was necessary to know the line shape from nonreacting $^9$Li projectiles. Thus we first subtracted a spectrum of projectiles, known *not* to react, from the total spectrum. These nonreacting projectiles, including both those which channeled in detector 7 and those which did not, had normal energy losses in detector 8 and were identified as $^9$Li in detectors 7–9. Tight gates on these parameters rejected some nonreaction events with large energy straggling, causing the small subsidiary peaks in the difference spectrum.

Except in the channeling region, the nonreaction yield outside the vertical dashed lines of Fig. 6(a) is negligible. Further, the difference spectrum in the channeling region connects smoothly with the reaction yield at lower and higher energies. Thus all events in the difference spectrum outside the dashed lines were counted as reactions, as were the interpolated events (under the solid line) beneath the peak. The latter events typically make up 3–5 % of the total reaction yield.

The events identified in spectra such as Fig. 6(a) were added to the $n$-removal events found by analyzing two-dimensional spectra, as described in Sec. III. The combined reaction probability $\eta_7$, for reactions occurring in detector 7 and all detectors and lead targets which precede it, is the ratio of the combined reaction yield to the incident flux. Section III D shows how $\sigma_R$ is found from $\eta_7$ and other data.

One concern was that elastically scattered projectiles

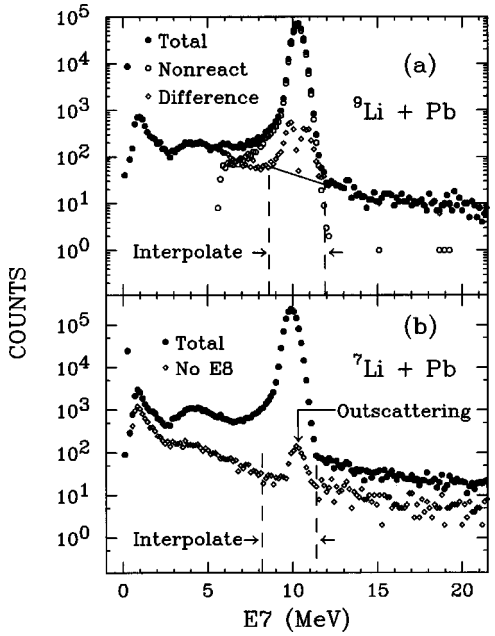


FIG. 6. (a) Energy-loss spectra of detector 7 with incident $^9$Li projectiles for all events, nonreaction events, and their difference interpolated to find reaction yield under the nonreaction peak. The $\sim 10^4$ events in a channel near zero energy are from reactions all of whose charged products stopped before detector 7. (b) Spectra for incident $^7$Li of all detector 7 events, and of those in anticoincidence with detector 8, showing signal due to events scattering out of detector 8.

might simulate reaction events by leaving the telescope, since detectors 8 and 9 had smaller areas than the others. We observed outscattering in spectra of detector 7, (where scattered projectiles have their maximum $dE/dx$) in anticoincidence with detector 8. A typical result is shown in Fig. 6(b). The outscattered events, for $^7$Li and all other projectiles, are inside the interpolation region and therefore cannot simulate reactions. The observed outscattering yield was 0.7% of the incident beam for $^6$Li and less for other projectiles.

## III. EXPERIMENTAL RESULTS

### A. 2*n* removal from $^{11}$Li

The $2n$-removal yield from $^{11}$Li included two contributions. Events from most of the telescope are identified *above* the normal-$\Delta E_7$ band (see Fig. 3); their $\Delta E_7$ spectrum is shown in Fig. 5(a). Figure 5(b) shows the $\Delta E_8 + \Delta E_9$ energy spectrum for all events *in* the band. The peak near 220 MeV includes some $2n$-removal events from the last Pb target, and a smaller number of $3n$- and $4n$-removal events. The deduced events in this peak lie above the solid interpolation line; dashed lines indicate the assigned uncertainty. After subtracting the $3n$- and $4n$-removal contributions (Sec. III C), the deduced $2n$ yield makes up $(24 \pm 5)\%$ of the total $2n$-removal yield. $^{11}$Li+Si events, for which $\sigma_{-2n} \simeq 0.4$ b [1], are about 5% of the observed $2n$-removal yield and, after subtraction, contribute negligibly to the experimental error.

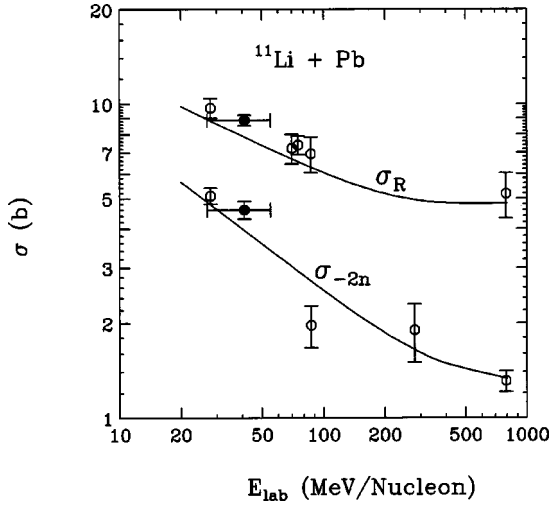


FIG. 7. $\sigma_R$ and $\sigma_{-2n}$ for $^{11}$Li+Pb vs energy. Filled data points are from this experiment and open data points are from Refs. [5–9]. Curves show microscopic calculations by Esbensen [11].

Events were lost if the $^9$Li fragment itself reacted later, or stopped before detector 8 due to its momentum transfer in the reaction. We estimated the detection efficiency by calculating the $\Delta E_7$ spectrum using the $\sigma_R$ for $^9$Li+Pb measured in this experiment and $\sigma_{-2n}$ obtained from Esbensen and Bertsch [11]. The fragment momentum distribution was assumed to be Lorentzian [12]

$$N(p)dp = \frac{2\Gamma p^2 dp}{\pi(\Gamma^2/4 + p^2)^2} \tag{2}$$

with isotropic emission in the $^{11}$Li c.m. system. We took $\Gamma$ to be 45 MeV/$c$ [13] and found the fragment detection efficiency to be $0.94 \pm 0.03$.

Interpolation and fragment-loss uncertainties were combined in quadrature to obtain a $\sigma_{-2n}$ of $4.4 \pm 0.3$ b averaged over the projectile energies (27 to 55 MeV/nucleon) in all four Pb targets. Figure 7 shows this and other known data for $2n$ removal from $^{11}$Li.

Uncertainties in extrapolation to determine the late fragmentation yield (i.e., events in the $\Delta E_7$ band) affect both our measured $\sigma_{-xn}$ and $\sigma_R$ data. Some fragments produced early in the telescope stop in detector 7 and therefore are not identified. However they are correctly counted in $\sigma_R$ since they give anomalous signals in one or more singles spectra including that of detector 7.

### B. 2*n* removal from $^6$He and $^8$He

In contrast to $^{11}\text{Li} \rightarrow {}^9$Li dissociation, only about half of the $\alpha$ particles from $^6$He dissociation reached detectors 7 and 8 for identification, due to their larger relative mass difference and the thicker Pb targets. Therefore, to find $\sigma_{-2n}$, we compared the expected $\alpha$ yield in the region between the normal-$\Delta E_7$ band and detector saturation (i.e., $E_\alpha$ between 6 and 18 MeV) with the yield predicted by a calculation similar to that described above for $^{11}$Li.

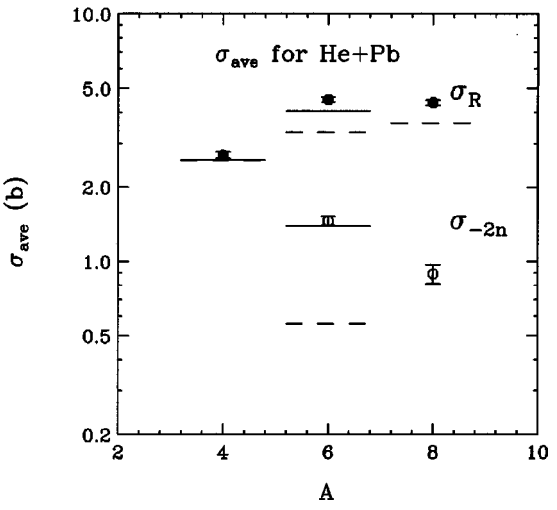


FIG. 8. Measured $\sigma_R$ (filled data points) and $\sigma_{-2n}$ (open data points) vs A for He isotopes on Pb, with microscopic predictions including Coulomb dissociation (solid horizontal lines) and neglecting it (dashed lines). The two $\sigma_R$ predictions for $^4$He are indistinguishable. Data are averaged over energy ranges given in Table I.

The basis of our $\sigma_{-2n}$ prediction is described in Sec. IV A. A momentum distribution parameter, $\Gamma = 120\,\mathrm{MeV}/c$, has been reported [12,14] only for a C target at 0.4 GeV/nucleon. The distribution must be narrower at our energy, since many forward-emitted fragments would not conserve energy if $\Gamma = 120\,\mathrm{MeV}/c$. We therefore used a renormalized distribution similar to Eq. (2), cut off at the largest momentum which conserved energy for those fragments. Fortunately the results are insensitive to $\Gamma$; when $\Gamma$ was varied from 40 to $120\,\mathrm{MeV}/c$ the predicted yield varied by only 3%. The ratio of observed to predicted events was $0.97 \pm 0.03$, increasing to $1.05 \pm 0.04$ after correction for beam attenuation before dissociation and fragment reactions afterwards. We thus obtained $\sigma_{-2n} = 1.46 \pm 0.06$ b.

Figure 4(a) shows the observed $\Delta E_7$ spectrum and the fit predicted with this calculation. Figure 4(b) shows the spectrum of incident energies at which $^6$He dissociates, predicted for the events detected both in and above the $\Delta E_7$ band. The mean dissociation energy for these events is 37 MeV/nucleon, with 80% of them lying between 28 and 52 MeV/nucleon.

For the $^8\mathrm{He} \rightarrow {}^6\mathrm{He}$ analysis we again varied $\Gamma$ from 40 to $120\,\mathrm{MeV}/c$, since the fragment momentum distributions from $^8$He and $^6$He on light targets at high energies [15,16] are similar. One source of uncertainty is that we have no predictions for $\sigma_{-2n}$ vs energy which include EMD. We analyzed the data assuming (a) no energy dependence and (b) the same dependence as for $^6$He. The latter seems more realistic since the energy dependence in the microscopic model is mainly that of the nucleon-nucleon cross section. Our result, $\sigma_{-2n} = 0.89 \pm 0.08$ b, is consistent with both analyses; 80% of the events occur for incident energies between 26 and 45 MeV/nucleon.

### C. Other neutron-removal reactions

We give only an estimate of $\sigma_{-4n}$ for $^8\mathrm{He} \rightarrow {}^4\mathrm{He} + 4n$, since the $^4$He have only a short range in the Pb targets and their momentum distributions are unknown. If we assume that the charged fragments are spectators (i.e., no momentum is transferred to them in the reaction), then all $^6$He's produced in the last two Pb targets are identified in detectors 7 through 9 while $\alpha$ particles are collected from only the last 1.5 mm of the last target. From the ratios of the identified yields and of the target thicknesses contributing to those yields, we found $\sigma_{-4n} \approx 0.5$ b. The $4n$-removal cross section for $^8$He+Si was also found, earlier, to be about half that for $2n$ removal [1]; that result too was approximate since it was found by decomposing the $n$-removal peak in the total energy spectrum.

Other $n$-removal cross sections are approximate, for similar reasons. All spectator $^8$Li fragments produced from $^{11}$Li in the four Pb targets, and about 70% of the spectator $^7$Li fragments, are identifiable. Their observed yield contributes 0.55 b to $\sigma_R$, leading to a combined cross section of about 0.7 b for removing 3 or 4 neutrons from $^{11}$Li. Similarly, the summed $n$-removal cross sections from both $^8$Li and $^9$Li are about 0.6 b and that from $^7$Li is about 0.1 b.

### D. Energy-averaged total reaction cross sections

The probability $\eta_3$ of a reaction occuring in any of the first 3 Si detectors is given by

$$1 - \eta_3 = \exp(-\sigma_{R,\mathrm{Si}} n_{\mathrm{Si}}), \tag{3}$$

where $\sigma_{R,\mathrm{Si}}$ is the energy-averaged total reaction cross section on Si and $n_{\mathrm{Si}}$ is the total nuclei per unit area in those detectors. Likewise $\eta_7$, the probability of a reaction in or before detector 7 is given by

$$1 - \eta_7 = \exp(-\sigma_{R,\mathrm{Pb}} n_{\mathrm{Pb}} + \sigma_{R,\mathrm{Si}} n_{\mathrm{Si}}), \tag{4}$$

where the exponential arguments include contributions from all Pb targets and the first seven detectors. Thus the total cross section on Pb, $\sigma_{R,\mathrm{Pb}}$, energy-averaged over all four targets, is

$$\sigma_{R,\mathrm{Pb}} n_{\mathrm{Pb}} = \ln[(1-\eta_3)/(1-\eta_7)] - \sigma_{R,\mathrm{Si}} n_{\mathrm{Si}}. \tag{5}$$

where $\sigma_{R,\mathrm{Si}} n_{\mathrm{Si}}$ refers to only detectors 4–7. Values of $\sigma_{R,\mathrm{Pb}}$ obtained for all projectiles are given in Table I and shown in Figs. 8 and 9. The uncertainty in $n_{\mathrm{Pb}}$ due to target nonuniformity was $\pm 2\%$; that for $n_{\mathrm{Si}}$ was negligible.

$\sigma_{R,\mathrm{Si}}$ was found by microscopic model calculations. The calculated $\sigma_{R,\mathrm{Si}}$'s for all projectiles are plotted vs energy in Figs. 3–5 of Ref. [1]. Predicted rather than measured values were used in Eq. (5), since the original Si data of Ref. [1] are at slightly different energies. Since these data could be fitted to an accuracy of $\pm 10\%$ by these calculations, we assigned 10% uncertainty to $\sigma_{R,\mathrm{Si}}$ in Eq. (5).

$\eta_7$ was found by adding the probability for $n$-removal reactions identified in detectors 7–9 to that for other reactions observed in the singles energy spectrum of detector 7. The uncertainty in the singles yield was taken to be $\frac{1}{3}$ of the interpolated counts (see Fig. 6); that for the $n$-removal reactions included error estimates for setting identification gates and interpolating into the normal-$\Delta E_7$ bands. This gave a

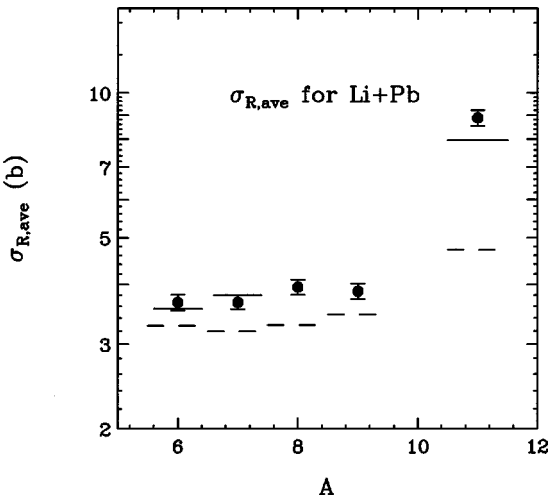


FIG. 9. Measured $\sigma_R$ vs A for Li isotopes on Pb, with microscopic predictions including Coulomb dissociation (solid horizontal lines) and neglecting it (dashed lines). Data are averaged over energy ranges given in Table I.

typical uncertainty of $\pm 3\%$ in the logarithmic term of Eq. (3) and was the largest source of experimental uncertainty.

$\eta_3$, found by microscopic calculations, was also generally consistent with the $\eta_3$ measured from this detector's singles spectrum. The uncertainty, taken to be the difference between measurement and calculation, was included in our error analysis but was always less than that in $\eta_7$. Measurements of $\eta_2$, the reaction probability in detector 2, also were consistent with microscopic calculations.

One uncorrected experimental error is our loss of inelastic scattering events to low-lying states in Pb, with the projectile remaining in its ground state. The group to the first excited state is generally the most prominent [17,18]. Integration of the inelastic angular distribution for 60*A* MeV $\alpha$ particles to this state in $^{208}$Pb [19] gives a cross section of about 0.02 b. Similar values for 35*A* MeV $^6$Li on $^{12}$C, $^{28}$Si, and $^{58}$Ni [18] are about 0.03 b with little dependence on the target A. These cross sections are smaller than our stated uncertainties in $\sigma_R$. Alternately, our data may be considered measurements of the interaction cross section $\sigma_I$, which includes all events in which *A* and/or *Z* of the projectile changes. Uncertainties due to counting statistics were negligible.

### E. $\sigma_R(E)$ for $^4$He and $^{6,7}$Li

Total reaction cross sections for these three isotopes, which have very small *n*-removal cross sections, were found for the projectile energy ranges in individual Pb sheets by a method similar to that of the last subsection. For example, $\eta_7$ in Eqs. (4) and (5) was replaced by $\eta_4$ to find $\sigma_R$ for the first Pb target. The results, shown in Fig. 10, have larger uncertainties than the four-target averages since the $\eta$'s in consecutive detectors have smaller differences. The results for $\alpha$+Pb are in excellent agreement with those of Ingemarsson *et al.* [20] at the energies where the data sets overlap. The lowest-energy $^6$Li datum agrees with the optical-model prediction of Nadasen *et al.* [21], which was obtained from precision measurements of large-angle elastic scattering.

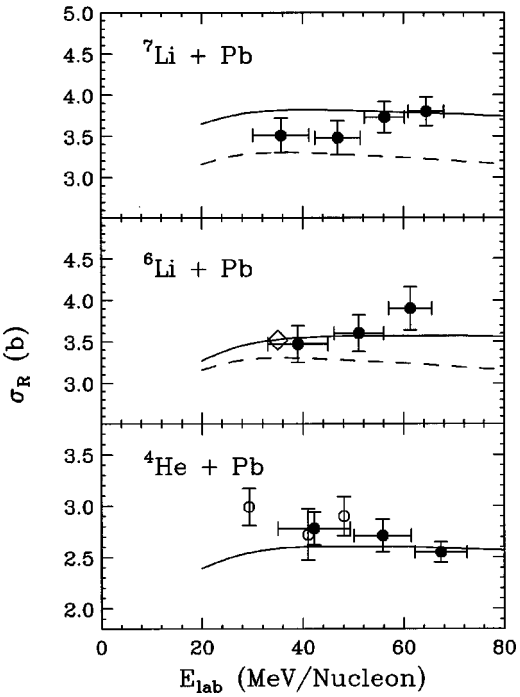


FIG. 10. Measured $\sigma_R$ vs energy (filled data points) for $^4$He, $^6$Li, and $^7$Li on Pb. Solid (dashed) curves show microscopic predictions including (neglecting) Coulomb dissociation. The diamond shows an optical model prediction of Ref. [21] for $^6$Li, and open data points show $^4$He+Pb data from Ref. [20]. Note the zero offsets of the vertical scales.

We report only the four-target average $\sigma_R$'s for other projectiles, since their *n*-removal cross sections are larger and of unknown energy dependence. Nevertheless these averages seem adequate for testing theoretical models, since the data of Fig. 10 and the microscopic calculations for all isotopes show only a weak energy dependence for $\sigma_R$ at these energies.

## IV. MICROSCOPIC MODEL PREDICTIONS

Previous measurements [1,2] on Si targets were analyzed in the context of a microscopic model which relates nuclear matter distributions and nucleon-nucleon interaction cross sections to $\sigma_R$ and $\sigma_{-2n}$ data. Therefore, for comparison, we interpret the present Pb data through similar calculations.

### A. Predictions of $\sigma_{-2n}$

$\sigma_{-2n}$ for $^6$He+Pb was calculated as before [22] except that we avoid using an arbitrary cutoff radius for EMD. The probability $\chi_{\rm val}(b)$ that the valence neutrons are not removed by the nuclear force, when the impact parameter is *b*, is

$$\chi_{\rm val}(b) = \exp\left[ -\sigma_{NN} \int ds \int \int \int \rho_{\rm val} \rho_t dV_t \right]. \qquad (6)$$

The valence neutron and target matter densities in target volume $dV_t$ are $\rho_{\rm val}$ and $\rho_t$. The nucleon-nucleon total cross

TABLE I. Measurements and microscopic predictions (in b) of $\sigma_R$ and $\sigma_{-2n}$ for He and Li isotopes on Pb.

| Type | Energy (MeV/nucleon) | Measurement (b) | Predictions no EMD (b) | Predictions with EMD (b) | Source |
|---|---|---|---|---|---|
| $^4$He, $\sigma_R$ | 35–73 | 2.69±0.08 | 2.56 | 2.57 | this work |
| $^6$He, $\sigma_R$ | 23–63 | 4.51±0.10 | 3.33 | 4.06 | this work |
| $^8$He, $\sigma_R$ | 19–53 | 4.38±0.11 | 3.62 | | this work |
| $^6$Li, $\sigma_R$ | 33–66 | 3.67±0.14 | 3.28 | 3.56 | this work |
| $^7$Li, $\sigma_R$ | 30–68 | 3.67±0.12 | 3.19 | 3.80 | this work |
| $^8$Li, $\sigma_R$ | 30–64 | 3.95±0.14 | 3.29 | | this work |
| $^8$Li, $\sigma_R$ | 72–90 | 3.01±1.85 | 3.17 | | Ref. [7] |
| $^9$Li, $\sigma_R$ | 29–60 | 3.87±0.14 | 3.46 | | this work |
| $^9$Li, $\sigma_R$ | 66–95 | 3.69±0.43 | 3.29 | | Ref. [7] |
| $^{11}$Li, $\sigma_R$ | 27–55 | 8.70±0.34 | 4.72 | 7.96 | this work |
| $^6$He, $\sigma_{-2n}$ | 28–52 | 1.46±0.06 | 0.56 | 1.39 | this work |
| $^8$He, $\sigma_{-2n}$ | 26–45 | 0.89±0.08 | | | this work |
| $^{11}$Li, $\sigma_{-2n}$ | 27–55 | 4.4±0.3 | 1.4 | 3.95 | this work |

section $\sigma_{NN}$ is obtained from the Charagi-Gupta prescription [23], and *ds* is an element of the trajectory. The core survival probability $\chi_{\rm core}$ is found by replacing $\rho_{\rm val}$ with $\rho_{\rm core}$ in Eq. (6). The $^6$He densities $\rho_{\rm core}$ and $\rho_{\rm val}$ were taken to be two-term harmonic oscillator form factors [24], and $\rho_t$ for Pb was a two-parameter Fermi (2pF) function [25]. The probability $P_{\rm nuc}(b)$ that nuclear forces remove the valence neutrons at impact parameter $b$ without disrupting the core is then

$$P_{\rm nuc}(b)=\chi_{\rm core}(b)[1-\chi_{\rm val}(b)]. \tag{7}$$

The probability $P_{\rm coul}(b)$ of EMD when nuclear forces affect neither core nor valence nucleons is

$$P_{\rm coul}(b)=\chi_{\rm core}(b)\chi_{\rm val}(b)(16\pi^3/9\hbar c)\int N(\epsilon_1;E,b) \times[dB(\epsilon_1;E)/dE]dE, \tag{8}$$

where the electric dipole response function $dB(\epsilon_1;E)/dE$ [26] and the virtual photon density $N(\epsilon_1;E,b)$ [22] are integrated over all $^6$He continuum energies. Finally we have

$$\sigma_{-2n}=2\pi\int [P_{\rm nuc}(b)+P_{\rm coul}(b)]bdb. \tag{9}$$

Our prediction for $\sigma_{-2n}$ vs energy appears in Fig. 4(b). The predicted cross section, averaged over the distribution shown, is 1.39 b, in agreement with our measurement of 1.46±0.06 b. The Coulomb cross section, i.e., the second term in Eq. (7), accounts for 60% of $\sigma_{-2n}$. In this decomposition, the nuclear cross section would equal $\sigma_{-2n}$ if Coulomb forces were ''turned off.'' To further test the method, we calculated $\sigma_{-2n}$ for $^6$He+Pb at 800*A* MeV to be 0.79 b, in agreement with the measurement of 0.85±0.05 b [27].

The predictions of both $\sigma_{-2n}$ and $\sigma_R$ for $^{11}$Li, shown in Fig. 7, are by Esbensen from a microscopic model [11] which includes the effect of spatial correlation between the two valence neutrons.

### B. Predictions of $\sigma_R$

We first included only nuclear interactions in microscopic calculations of $\sigma_R$ for all projectiles, as in Ref. [1], with projectile densities taken from Ref. [1]. The results (Table I) are too low for nearly all projectiles; that for $^{11}$Li is too low by a factor of 2. This conclusively demonstrates the need to include EMD effects for all projectiles except $^4$He, which was shown [28] to have an EMD cross section of less than 1% of $\sigma_R$. The previously cited $2pF$ form factor [25] was used for the Pb target density. When instead the Pb density-functional form factors of Fayans *et al.* [29] were used, the predictions changed by less than 1%.

Table I shows that similar calculations agree with $\sigma_R$ measurements for $^{8,9}$Li+Pb at slightly higher energies [7], within the larger uncertainties of those data. Strong absorption (SA) calculations using the formulas of Shen *et al.* [30] gave $\sigma_R$'s 25% lower for $^{11}$Li, and 5 to 10% lower for other projectiles, than the microscopic calculations; thus, they underpredict the $^{11}$Li measurement by about 60%. Somewhat better SA results were obtained for the same projectiles on Si [1]. For the Pb target we cannot expect good fits since the SA model does not explicitly include EMD.

Microscopic predictions including EMD effects are given in Table I for projectiles whose photodissociation cross sections or electric dipole response functions are known. For $^6$He, in analogy to Eq. (7),

$$\sigma_R=2\pi\int [1-\chi_{{\rm val}(b)}\chi_{\rm core}(b)+P_{\rm coul}(b)]\ bdb. \tag{10}$$

Measured photodisintegration cross sections were used to include EMD for $^6$Li and $^7$Li, as described for $^4$He in Ref.

[29]. Since the virtual photon density falls rapidly with increasing $E_\gamma$, only photodissociation reactions which are prolific near the lowest threshold were needed; these are $(\gamma,xn)$ for both $^{6,7}$Li [31] and $(\gamma,t)$ for $^{7}$Li [32]. Esbensen [11] provided the $\sigma_R$ for $^{11}$Li.

The measured $\sigma_R$ is at least as large for $^{6}$He as for $^{8}$He. One explanation is that $\sigma_{-2n}$ is at least 50% larger for $^{6}$He, and 60% of the $^{6}$He $\sigma_{-2n}$ comes from EMD, which must be larger for $^{6}$He since the last two neutrons are less tightly bound.

An intuitively appealing subtraction relationship for $2n$-halo nuclei, e.g.,

$$\sigma_{-2n}(^{11}\mathrm{Li}) = \sigma_R(^{11}\mathrm{Li}) - \sigma_R(^{9}\mathrm{Li}), \tag{11}$$

was proposed by Ogawa *et al.* [33] and found to agree with high-energy data. The equality holds when reactions of the halo nucleus include only core reactions and $2n$ removal. The $\sigma_R$ data of Table I yield $4.83 \pm 0.37$ b for the right-hand side of Eq. (11), agreeing with our measurement $\sigma_{-2n}(^{11}\mathrm{Li}) = 4.4 \pm 0.3$ b. However, the $^{9}$Li and $^{11}$Li cross sections are measured for slightly different energy ranges. We therefore adjusted the $^{9}$Li $\sigma_R$ by assuming that its energy dependence follows the microscopic prediction; Eq. (9) then yields $\sigma_{-2n} = 4.81 \pm 0.37$ b. For $^{6}$He, we predict $\sigma_{-2n} = 1.82 \pm 0.13$ b from the original data and $1.86 \pm 0.13$ b with the energy adjustment, exceeding our measurement of $1.46 \pm 0.06$ b by more than 2 standard deviations. The discrepancy may result from motion of the $^{4}$He core relative to the $^{6}$He c.m., caused by the Fermi motion of the valence neutrons [34]. This would increase the effective size of the core and, therefore, the $\sigma_R$ of $^{6}$He. This effect is larger for $^{6}$He than for $^{11}$Li, owing to the greater mass and smaller binding energy of $^{11}$Li.

## V. CONCLUSIONS

Measurement of $\sigma_R$ by placing Pb target foils between thin Si detectors seems capable of 5% accuracy, and therefore can generate data adequate for testing theoretical models. The success of the method shows that Si telescope measurements of $\sigma_R$ for other solid targets are also feasible. Therefore, measurements on intermediate-mass targets would now be useful for testing the $Z$ dependence of EMD cross sections, which is model dependent [9]. Studies on light targets (Be or C) would give more sensitive measurements of the projectile rms radii. A further justification for $\sigma_R$ measurements at energies below 60 MeV/nucleon is that the large nucleon-nucleon interaction cross section at these energies increases the sensitivity of $\sigma_R$ to the matter density in the halo region [2].

We offer the following suggestions for related theoretical studies. Electric dipole response functions for $^{8}$He, $^{8}$Li, and $^{9}$Li are needed to resolve the discrepancies between measured and predicted microscopic $\sigma_R$'s for these nuclei. Al Khalili *et al.* [35] showed that microscopic calculations using static densities underestimate the radii of halo nuclei, and three-body correlations must be included for a correct treatment. Their method was applied to the high-energy data; an adaptation to our energies would now be of interest. Finally, microscopic calculations in which nucleon-target optical potentials replace nucleon-nucleon cross sections, as performed by Hencken *et al.* [36] for the fragment momentum distributions from $^{8}$B and $^{11}$Be, would be welcome.

## ACKNOWLEDGMENTS

We thank Henning Esbensen, Sergei Fayans, Peter Schwandt, Ian Thompson, and Dave Youngblood for their advice and interest, and for sending us results of their calculations and measurements. We also thank Mu-Young Lee, Tom O'Donnell, K. A. G. Rao, Dan Sisan, and Bill Yuhasz for their help in setting up and running the experiment. The Howard Hughes Medical Institute and the McGregor-Oresman Fund supported the work of Megan McKinnon and Nathan Shaner. The work was also supported by the National Science Foundation under Grants No. PHY-9722604 and PHY-9804869 (UM-Ann Arbor), PHY-9602869 (UM-Dearborn), PHY-9528844 (NSCL), PHY-9401761 (Notre Dame), and PHY-9423659 (Oberlin).

[1] R. E. Warner *et al.*, Phys. Rev. C **54**, 1700 (1996), and references therein.
[2] R. E. Warner *et al.*, Phys. Rev. C **52**, R1166 (1995); R. E. Warner *et al.*, Nucl. Phys. **A635**, 292 (1998).
[3] G. F. Bertsch, B. A. Brown, and H. Sagawa, Phys. Rev. C **39**, 1154 (1989).
[4] R. E. Warner and G. N. Felder, Phys. Rev. C **42**, 2252 (1990).
[5] D. Sackett *et al.*, Phys. Rev. C **48**, 118 (1993).
[6] S. Shimoura, in *Proceedings of the International Symposium on Structure and Reactions of Unstable Nuclei*, Niigata, Japan 1991, edited by K. Ikeda and Y. Suzuki (World Scientific, Singapore 1991), p. 132.
[7] B. Blank *et al.*, Nucl. Phys. **A555**, 408 (1993); Z. Phys. A **340**, 41 (1991).
[8] F. Humbert *et al.*, Phys. Lett. B **347**, 198 (1995).
[9] T. Kobayashi *et al.*, Phys. Lett. B **232**, 51 (1989).
[10] J. P. Biersack and J. F. Ziegler, Computer code TRIM, version 91.14, 1992 (unpublished).
[11] H. Esbensen and G. F. Bertsch, Phys. Rev. C **46**, 1552 (1992); H. Esbensen (private communication).
[12] P. G. Hansen, A. S. Jensen, and B. Jonson, Annu. Rev. Nucl. Sci. **45**, 591 (1995).
[13] K. Riisager, in *Proceedings of the Third International Conference on Radioactive Nuclear Beams*, East Lansing, MI, 1993, edited by D. J. Morrissey (Editions Frontieres, Gif-sur-Yvette, 1993), p. 285.
[14] T. Kobayashi, Nucl. Phys. **A538**, 343c (1992).
[15] T. Kobayashi, O. Yamakawa, K. Omata, K. Sugimoto, T. Shimoda, N. Takahashi, and I. Tanihata, Phys. Rev. Lett. **60**, 2599 (1988).
[16] T. Nilsson *et al.*, Nucl. Phys. **A598**, 418 (1996).
[17] J. Alster, Phys. Lett. **25B**, 459 (1967); Phys. Rev. **141**, 1138

(1966).
[18] A. Nadasen, M. McMaster, M. Fingal, J. Tavormina, J. S. Winfield, R. M. Ronningen, P. Schwandt, F. D. Becchetti, J. W. Jänecke, and R. E. Warner, Phys. Rev. C **40**, 1237 (1989).
[19] D. H. Youngblood (private communication).
[20] A. Ingemarsson *et al.*, Nucl. Phys. A (to be published).
[21] A. Nadasen, M. McMaster, M. Fingal, J. Tavormina, P. Schwandt, J. S. Winfield, M. F. Mohar, F. D. Becchetti, J. W. Jänecke, and R. E. Warner, Phys. Rev. C **39**, 536 (1989).
[22] R. E. Warner, Phys. Rev. C **55**, 298 (1997).
[23] S. K. Charagi and S. K. Gupta, Phys. Rev. C **41**, 1610 (1990).
[24] I. Tanihata, D. Hirata, T. Kobayashi, S. Shimoura, K. Sugimoto, and H. Toki, Phys. Lett. B **289**, 261 (1992).
[25] C. W. de Jager, H. de Vries, and C. de Vries, At. Data Nucl. Data Tables **14**, 479 (1974).
[26] B. V. Danilin, I. J. Thompson, M. V. Zhukov, and J. S. Vaagen, Nucl. Phys. **A632**, 383 (1998); I. J. Thompson (private communication).
[27] I. Tanihata, Nucl. Phys. **A522**, 275c (1991).
[28] R. E. Warner, M. H. McKinnon, H. Thirumurthy, and A. Nadasen, Phys. Rev. C **59**, 1215 (1999).
[29] S. A. Fayans, E. L. Trykov, and D. Zawischa, Nucl. Phys. **A568**, 523 (1994); S. Fayans (private communication).
[30] W.-Q. Shen, B. Wang, J. Feng, W.-L. Zhan, Y.-T. Zhu, and E.-P. Feng, Nucl. Phys. **A491**, 130 (1989).
[31] S. S. Dietrich and B. L. Berman, At. Data Nucl. Data Tables **38**, 199 (1988).
[32] D. M. Skopic, J. Asai, E. L. Tomusiak, and J. J. Murphy II, Phys. Rev. C **20**, 2025 (1979).
[33] Y. Ogawa, K. Kabana, and Y. Suzuki, Nucl. Phys. **A543**, 722 (1992).
[34] J. A. Tostevin, J. S. Al-Khalili, M. Zahar, M. Belbot, J. J. Kolata, K. Lamkin, D. J. Morrissey, B. M. Sherrill, M. Lewitowicz, and A. H. Wuosmaa, Phys. Rev. C **56**, R2929 (1997).
[35] J. S. Al-Khalili, J. A. Tostevin, and I. J. Thompson, Phys. Rev. C **54**, 1843 (1996).
[36] K. Hencken, G. F. Bertsch, and H. Esbensen, Phys. Rev. C **54**, 3043 (1996).